NRL Report 6600

Investigation of Solid/Liquid Interface Temperatures via Isenthalpic Solidification

M. E. Glicksman and R. J. Schaefer

Metal Physics Branch
Metallurgy Division

October 13, 1967

APPROVED FOR PUBLIC RELEASE - DISTRIBUTION UNLIMITED

NAVAL RESEARCH LABORATORY
Washington, D.C.

NRL Report 6600

Investigation of Solid/Liquid Interface Temperatures via Isenthalpic Solidification

October 13, 1967

NAVAL RESEARCH LABORATORY
Washington, D.C.

This document has been approved for public release and sale; its distribution is unlimited.

This page intentionally left blank.

CONTENTS

Abstract	iv
Problem Status	iv
Authorization	iv
INTRODUCTION	1
THEORY	1
Thermodynamics	1
Kinetics	3
EXPERIMENTAL TECHNIQUES	5
Establishment of the Transition Temperature	5
Light Scattering During Solidification	6
Speed of Solidification	8
DATA ANALYSIS	10
Planar Growth Hypothesis	10
Analysis for Nonplanar Growth	10
Determination of Interface Temperature	13
Interface Kinetics for P_4	14
SUMMARY	18
ACKNOWLEDGMENT	18
REFERENCES	18

ABSTRACT

Isenthalpic solidification of a pure supercooled liquid is shown to result in either a two-phase solid/liquid mixture in invariant equilibrium or a single-phase, totally solid material in univariant equilibrium, depending on the level of supercooling prior to solidification. The critical supercooling above which univariant equilibrium is obtained is large for metals (hundreds of centigrade degrees) but much smaller for certain molecular substances. Experiments on white phosphorus (alpha P_4) show that the critical supercooling (25.6 C°) can be reached, and exceeded, easily. Solidification rate measurements taken above and below the critical supercooling for P_4 show that the solid/liquid interface temperature varies smoothly with melt supercooling, although light-scattering experiments indicate that rapid changes occur in the extent of the dendritic zone as the critical supercooling is approached and exceeded.

A method for extracting interface attachment kinetics from solidification rate data was examined in detail and applied to our rate measurements on P_4. We find that above about 9 C° supercooling, P_4 solidifies with linear attachment kinetics having a rate constant of 17.7 ± 0.4 cm/sec C°. Below about 1 C° supercooling, P_4 solidifies with a faceted morphology indicative of layer-passage limited kinetics. Between 1 C° and 9 C° supercooling, transitional growth kinetics occur. These results are in qualitative agreement with the crystal growth theory of Cahn, et al., which predicts that attachment kinetics should change as the driving force for crystal growth is varied by substantial amounts.

PROBLEM STATUS

This report completes one phase of the problem; work on other aspects of the problem is continuing.

AUTHORIZATION

NRL Problem M01-10
Project RR 007-01-46-5408
and ARPA Order 418

Manuscript submitted June 5, 1967.

INVESTIGATION OF SOLID/LIQUID INTERFACE TEMPERATURES VIA ISENTHALPIC SOLIDIFICATION

INTRODUCTION

Recently, several successful experimental approaches have been described in which slowly advancing, complex dendritic interfaces in freezing organic compounds (1,2) and metals (3,4) were analyzed on the basis of *in situ* microscopic observation. Because the solidification speeds reported in those studies were near the lower limit for dendritic growth (e.g., $\sim 10^{-2}$ cm/sec in pure metals), the results were analyzable solely on the basis of heat-flow theory for isolated dendrites; no consideration was given to atomic attachment processes at the solid/liquid interface. Hamilton and Seidensticker (5) have reported on an excellent technique for estimating the growth kinetics of germanium dendrites growing in the speed range 0.1 to 1 cm/sec. Their technique is applicable to materials in which single dendrites or ribbon crystals can be grown under near steady-state conditions. These successes notwithstanding, no suitable method has yet been demonstrated for estimating the solidification kinetics of substances that solidify by rapid dendritic growth in the speed range 10 to 10^4 cm/sec. The lack of success in this area is perhaps not surprising considering our ignorance about the morphological details of the solid/liquid interface, which is topographically complex and advancing at high speed. Without this precise morphological information, a reliable estimate cannot ordinarily be made concerning the departure of interface temperature from the local equilibrium temperature; consequently, a kinetic relationship cannot be established between the magnitude of this temperature departure, which is the driving force for the molecular processes of solidification, and the speed of advance of the interface normal to itself, which is the local kinetic rate of solidification.

The purpose of this report is to present an approach to the problem of obtaining information on the kinetics of rapid solidification processes. Specifically, an analysis of solidification at extreme levels of supercooling will be presented which yields a method for establishing limits on the solid/liquid interface temperature at the kinetically most active regions of the interface. Several experiments on supercooled white phosphorus will then be described which provide a basis for the theoretical analysis and which yield quantitative kinetic data on molecular attachment processes during rapid solidification.

THEORY

Thermodynamics

Consider a uniformly supercooled pure melt thermally isolated from its surroundings. The initial (metastable) equilibrium state of this system is characterized thermodynamically by a single phase (liquid) at temperature T_0 and at (applied) pressure P_0. If solidification then occurs in the supercooled melt, the system will, given enough time, approach a final equilibrium state which is isenthalpic to the initial state. In other words, the assumed conditions of constant pressure and adiabatic isolation of the freezing system require that the enthalpies of the initial and final equilibrium states be equal. The type of postsolidification equilibrium is restricted to the two cases predicted from Gibbs' phase rule for a unary (one-component) system: (a) invariant equilibrium, where the final state is characterized by two phases (solid and liquid, at pressure P_0), at their *invariant* final temperature $T_f = T_e$, where T_e denotes the usual equilibrium temperature

between solid and liquid, and (b) univariant equilibrium, where the final state is characterized by one phase (solid, at pressure P_0) at a temperature $T_f < T_e$, where here T_f is some function of the initial temperature T_0.

The relationships between the thermodynamic states before and after isenthalpic solidification are indicated in Fig. 1. Figure 1 is a normalized enthalpy-temperature diagram in which the ordinate is the usual enthalpy function divided by the latent heat of fusion λ_0* and the abscissa is the absolute temperature divided by λ_0/C_ℓ, where C_ℓ is the specific heat (at constant pressure) of the liquid, assumed temperature independent. In such a representation the (normalized) enthalpy-temperature relation for the liquid phase will always be a straight line of unit slope, whereas the (normalized) enthalpy-temperature relation for the solid phase will in general be a curve with every point displaced vertically from the liquid enthalpy line by an amount λ/λ_0. Here, λ is the latent heat of fusion, which, in general, has a slight temperature dependence. As indicated in Fig. 1, a liquid phase at temperature ϑ_0 can exist in any of three types of contiguous, initial states: a stable state ($\vartheta_0 > \vartheta_e$), where no solidification can occur; a metastable, *undercooled* state ($\vartheta_e - 1 < \vartheta_0 < \vartheta_e$), where isenthalpic solidification produces invariant equilibrium at temperature $\vartheta_f = \vartheta_e$; and a metastable, *hypercooled* state ($\vartheta_0 < \vartheta_e - 1$), where isenthalpic solidification produces univariant equilibrium at temperature $\vartheta_f = \vartheta_0 + \lambda/\lambda_0$. The two metastable states are, therefore, distinguishable on the basis of whether the initial bath supercooling, $\Delta\vartheta \equiv \vartheta_e - \vartheta_0$, is less than unity (undercooled) or greater than unity (hypercooled). The effect of the initial state on the kinetics of freezing will now be considered.

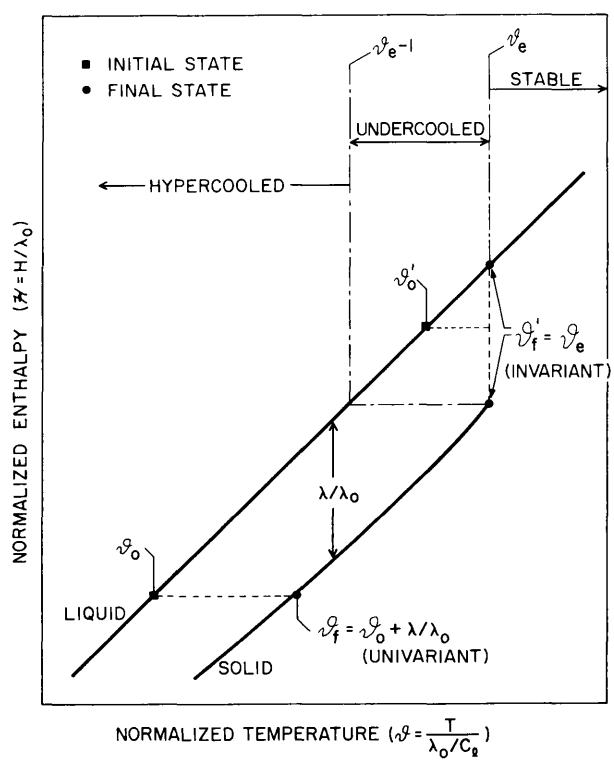

Fig. 1 - Normalized enthalpy-temperature diagram. Isenthalpic solidification reactions are indicated by the initial (■) and final (●) states of the system. Invariant equilibrium obtains for the initial condition $\vartheta_e - 1 < \vartheta_0' < \vartheta_e$, whereas univariant equilibrium obtains for the initial condition $\vartheta_0 < \vartheta_e - 1$. Above temperature ϑ_e, the liquid phase is stable relative to the solid phase.

*λ_0 is the latent heat of fusion at the equilibrium melting point ϑ_e.

Kinetics

So far, only the thermodynamic relationships for the equilibrium states before and after isenthalpic solidification have been considered. We now will discuss some possible kinetic processes that a solidifying system might undergo as it departs from the initial (metastable) equilibrium state and approaches a final equilibrium state.

Planar Solidification at Constant Speed - Figure 2a represents a system, initially supercooled an amount $\Delta\vartheta = \vartheta_e - \vartheta_0$, solidifying under isenthalpic conditions with a planar solid/liquid interface advancing at a constant rate V. The isenthalpic condition implies that no transfer of heat can occur between the system and its surroundings. If we assume that the thermophysical constants of the solid and liquid phases are independent of temperature, then an exact solution exists for the steady-state temperature distribution along the direction of growth, viz.,

$$\vartheta(X) = \vartheta_0 + \left[\Delta\vartheta \left(1 - \frac{C_\ell}{C_s}\right) + \frac{C_\ell}{C_s} \right] \exp(-VX/\alpha), \quad X \geq 0, \tag{1a}$$

(see Fig. 2b) and

$$\vartheta(X) = \vartheta_0 + \left[\Delta\vartheta \left(1 - \frac{C_\ell}{C_s}\right) + \frac{C_\ell}{C_s} \right] \qquad X \leq 0, \tag{1b}$$

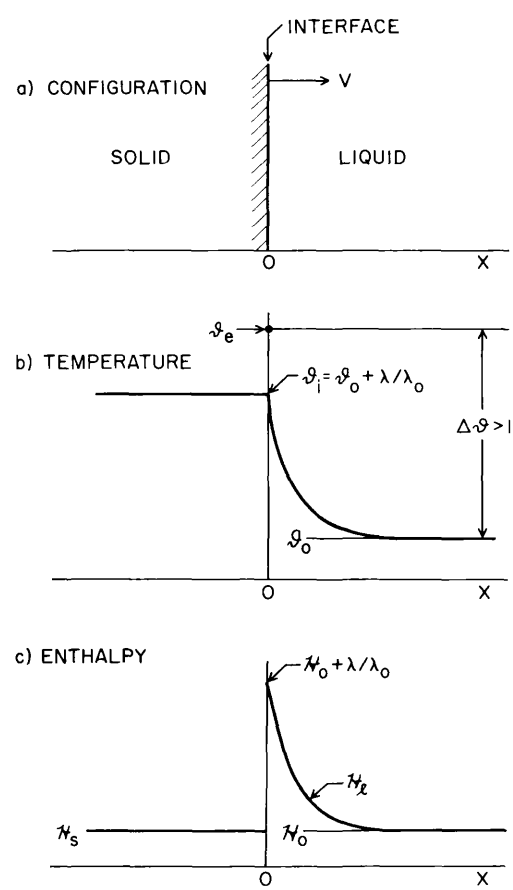

Fig. 2 - Isenthalpic solidification with a plane-front morphology: (a) steady-state configuration of the system near the solid/liquid interface; X = 0 denotes interface in a moving coordinate system; (b) normalized temperature versus distance in the vicinity of X = 0--note that the melt supercooling ($\Delta\vartheta$) must exceed unity as a necessary condition for this solidification mode; (c) normalized enthalpy versus distance near X = 0--note that the enthalpy of the solid is equal to that of the liquid far from the interface. Here, λ/λ_0 is substituted for the equivalent expression $[\Delta\vartheta(1 - C_\ell/C_s) + C_\ell/C_s]$ appearing in Eqs. (1a) and (1b).

where X is the distance to any point measured normal to the solid/liquid interface (X = 0) on a coordinate system moving with the solid/liquid interface. We will now make the approximation $C_s = C_\ell$, so the quantity within the brackets of Eqs. (1a) and (1b) becomes unity, and the expressions agree with those given in Refs. 6 and 7. The speed of advance V of the interface is a constant determined by the interface supercooling through some independent kinetic relationship of the general form

$$V = f[\vartheta_e - (\vartheta_0 + 1)] = f(\delta) . \tag{2}$$

Here, the interface supercooling δ is related to the melt temperature by the relation $\delta = \vartheta_e - (\vartheta_0 + 1)$. [See Fig. 3 for the scale of (normalized) supercooling used throughout this report.]

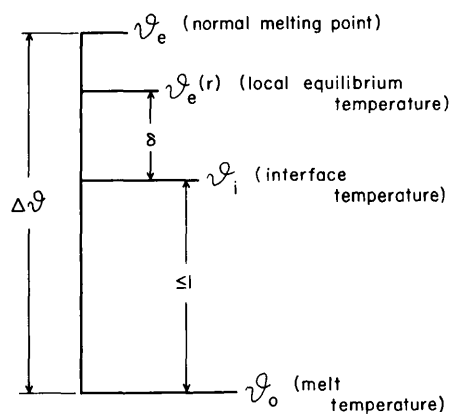

Fig. 3 - Reference scale of normalized temperatures and normalized temperature differences. All quantities shown are dependent or independent variables except ϑ_e which is a constant.

It becomes apparent from the nature of the heat-flow solutions, Eqs. (1a) and (1b) that steady-state advance of a planar solidification front under isenthalpic conditions requires an initial level of normalized supercooling, $\Delta\vartheta = \vartheta_e - \vartheta_0$, greater than unity; i.e., initially, the melt must be in a hypercooled state. Moreover, as is seen in Fig. 2c, the solid and liquid phases far ahead of and behind the transformation front have equal enthalpy. Thus, the solidification of a hypercooled melt ($\Delta\vartheta > 1$) via steady-state plane-front transformation appears to be a unary analog to the so-called massive transformations occurring without change of composition in binary systems (8).

In summary, the planar-front solidification just discussed represents the limiting case of isenthalpic solidification, wherein the temperature of every point on the solid/liquid interface is a constant amount (unity) above the melt temperature ϑ_0 at infinity; i.e., $\vartheta_i = \vartheta_0 + 1$. The interface in this case is spatially and temporally isothermal, but the rate of motion is determined by *both* heat-flow and kinetic considerations.

Nonplanar Solidification in Hypercooled Melts - The instabilities which lead to the breakdown of a planar solidification front should be operative in hypercooled systems as well as in normally undercooled systems. For instance, Figs. 4a and 4b are illustrations of nonplanar interfaces in a normally undercooled melt — where dendrites form — and in a hypercooled melt — where "scallops" form. "Scalloping" of the interface leads to the same type of enhanced heat diffusion that dendrites permit, but, with a scalloped interface, *total* solidification occurs some distance back from the most advanced regions of the interface. It will be shown later (with light-scattering experiments) that in the case of phosphorus the extent of the scalloped region diminishes rapidly with increased supercooling. Also, as the supercooling increases beyond about $\Delta\vartheta > 2$, the scalloped interface becomes, from a morphological standpoint, almost indistinguishable from a planar

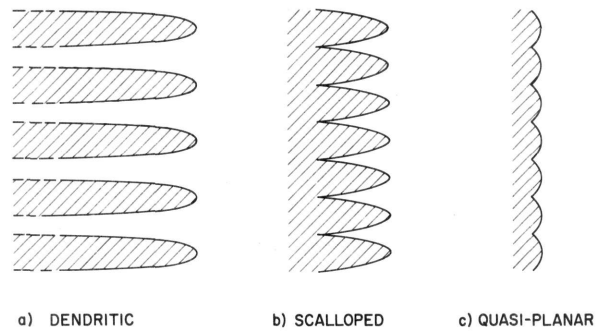

Fig. 4 - Nonplanar solidification morphologies: (a) dendritic, for undercooled melts, (b) scalloped, and (c) quasi-planar, for hypercooled melts. All three morphologies have complex thermal diffusion fields associated with their propagation.

interface. Thus, as the supercooling in a pure melt increases beyond unity, a continuous transition from dendritic, to scalloped, to quasi-planar* interfaces occurs, c.f., Fig. 4.

EXPERIMENTAL TECHNIQUES

White phosphorus (P_4) was chosen for study because its thermophysical properties are favorable for achieving large levels of (normalized) supercooling. Specifically, a normalized supercooling of unity is reached when liquid P_4 is cooled about 25 C° below its equilibrium temperature, $T_e = 44°C$;† by comparison, most metals require 300 C° to 500 C° cooling below their respective T_e's to reach unit normalized supercooling. In addition, the low entropy of fusion (9) of P_4 makes it likely that some aspects of its solidification behavior are similar to those of the pure metals (10).

Establishment of the Transition Temperature

A detailed description of the apparatus and experimental techniques used in determining the transition temperature between invariant and univariant isenthalpic solidification in P_4 has been given elsewhere (11). It will serve the purpose of this report, however, to repeat some of those results which are pertinent here. Figure 5 is a plot of measured postrecalescence temperature T_f versus initial melt temperature T_0 for a specimen of vacuum distilled P_4 undergoing isenthalpic solidification. The data shown in Fig. 5 exhibit a sharp slope discontinuity at $T_0 = 18.4°C$. In the temperature range $18.4°C < T_0 < 44°C$ the solidification was of the normal invariant type; i.e., the postrecalescence temperature was independent of the initial temperature and was always equal to the (invariant) equilibrium temperature T_e. However, for $T_0 < 18.4°C$ the postrecalescence temperature failed to reach T_e — falling short about 1.06 C° for each additional degree of initial supercooling. This latter behavior is, of course, characteristic of univariant solidification, where T_f is a function of T_0. This experiment served to

*The term quasi-planar denotes macroscopic planarity of the interface, but on the microscopic scale of the heat-flow the interface does not necessarily behave as a plane front.

†The symbol C° indicates a temperature interval, and the symbol °C indicates a specific temperature.

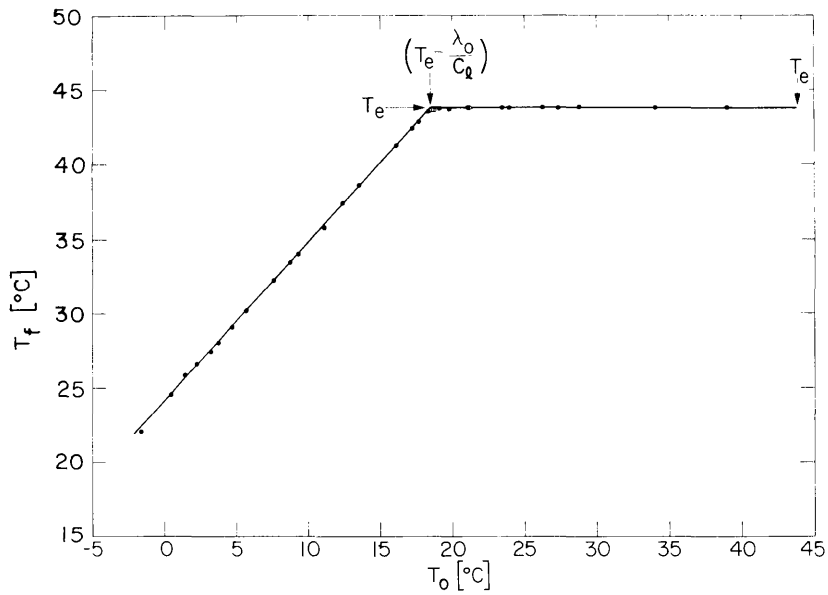

Fig. 5 - Final temperature T_f, established after isenthalpic solidification of supercooled liquid phosphorus, versus initial temperature T_0 of the molten phosphorus. The equilibrium temperature T_e is 44°C, and, as denoted by the sudden change in slope, the critical temperature for univariant solidification $T_e - \lambda_0/C_\ell$ is 18.4 ± 0.1°C.

establish unequivocally the minimum level of supercooling required for univariant isenthalpic solidification as $\Delta T_{min} = 25.6\ C°$.

Light Scattering During Solidification

An apparatus was constructed to permit an evaluation of structural changes during solidification in both the undercooled and hypercooled temperature ranges, viz., T_0 above and below 18.4°C, respectively. This apparatus consisted of a light-tight structure containing a stabilized collimated light source, a highly sensitive rapid-response CdS photodetector and readout circuitry, a specimen chamber, and a "trigger" mechanism for inducing solidification in the P_4 specimen at any desired level of supercooling. An experiment consisted of measuring the light intensity transmitted by a specimen of supercooled liquid P_4 and then monitoring the changes in transmitted intensity as freezing took place. The change in transmitted light intensity was caused by scattering of the main beam on solid/liquid and solid/solid interfaces that formed within the specimen. Thus, the decrease in transmitted light intensity was related to the average density of internal interfaces along the light path. Figure 6 is a composite diagram of scattered light intensity versus time, for various initial temperatures. Just prior to "triggering" solidification in each experiment (t = 0 min), the transmitted light intensity was adjusted to an arbitrary scale of 100, or, equivalently, the scattered light intensity was set to zero on an arbitrary scale of 100. Thus, all the curves of Fig. 6 have common ordinate and abscissa axes. Because the incident beam intensity was held constant during solidification, it is most convenient to think of the ordinate scale in Fig. 6 as proportional to the density of scattering sites present during freezing.

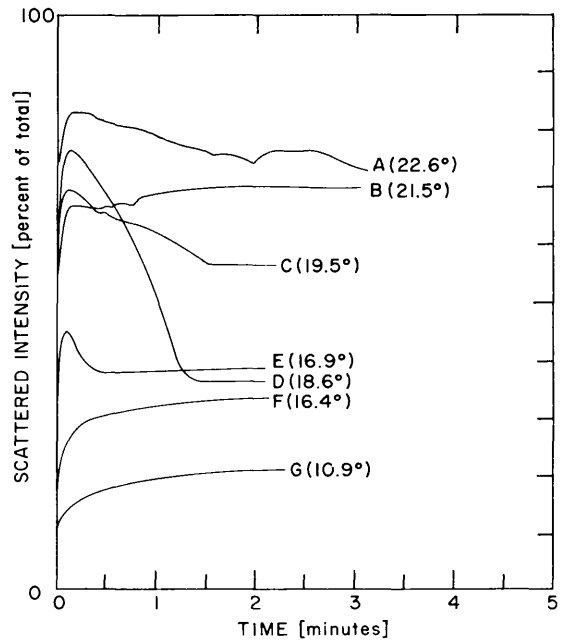

Fig. 6 - Percent scattered light intensity versus time after initiation of solidification in supercooled P_4. Curves A, B, C, and D are for undercooled melts with progressively increasing supercooling. Curves E, F, and G are for hypercooled melts with progressively increasing supercooling. Note the rapid change in behavior as the initial temperature drops below the critical temperature for univariant isenthalpic solidification (18.4°C).

We see, starting with the least undercooled (warmest) melts (curves A and B), that freezing caused a rapid increase in scattering sites, followed, thereafter, by only slight and somewhat irregular changes. This is typical of normal dendritic freezing, where the finely dispersed solid/liquid interfaces formed during passage of the main solidification front persist for relatively long times. If the system were truly adiabatic, the solid/liquid mixture would, in time, coarsen slightly, and the scattered intensity would diminish very slowly. Some heat losses and further solidification, however, were unavoidable over the period of the experiment (usually 3 to 5 min), and the decrease in scattering sites (solid/liquid interface area) accompanying this additional (nonisenthalpic) solidification accounts for the behavior of these curves. For specimens frozen at 19.5°C and, even more pronounced, for those frozen at 18.6°C, the scattering-site density shows a conspicuous maximum followed by a rapid decrease to a nearly constant level. This behavior is characteristic of systems solidifying from liquids with normalized supercooling near unity, where the enthalpy of the liquid phase at the initial temperature is approximately equal to the final enthalpy of the solid phase at the equilibrium temperature. Just after passage of the main solidification front, a transitory solid and liquid structure exists containing numerous pockets of interdendritic liquid; subsequently, these liquid regions solidify more or less rapidly by transferring their heat of fusion *locally* to the solid phase. This secondary solidification process leads to a dramatic decrease in the number of scattering sites, and either goes to completion (if the initial supercooling was slightly greater than unity) or stops when the system finally reaches the equilibrium temperature (if the initial supercooling was slightly less than unity).

As the initial normalized supercooling of the specimen rises above unity, that is, as hypercooling begins, the maximum in the scattered light intensity diminishes in amplitude and width, until in the case of the curves for temperatures below 16.9°C, the maxima are no longer resolved on the scale used in Fig. 6. The solidification structures responsible for the lower curves (F, G) are qualitatively similar to those responsible for curves D and E, except that no interdendritic liquid persists in the structures. Instead, it appears that the dendritic nature of the solidification must be confined to a fairly narrow zone just behind and moving with the main solidification front. This last case of freezing in a pure hypercooled liquid corresponds to what was previously termed a scalloped interface (Fig. 4).

Speed of Solidification

Figure 7 is a diagram of the apparatus employed in measuring the linear rates of solidification in supercooled liquid P_4. Two tungsten-Kovar-A thermocouples (W_1/K_1 and W_2/K_2) were used to determine the specimen's temperature prior to freezing and to verify that no appreciable temperature gradients existed along the 10-cm growth path. To measure the time for the solidification front to traverse the growth path, the two thermocouples were connected in series (opposing polarity) as a differential thermocouple, the output signal from which, after suitable preamplification, was displayed on an oscilloscope.

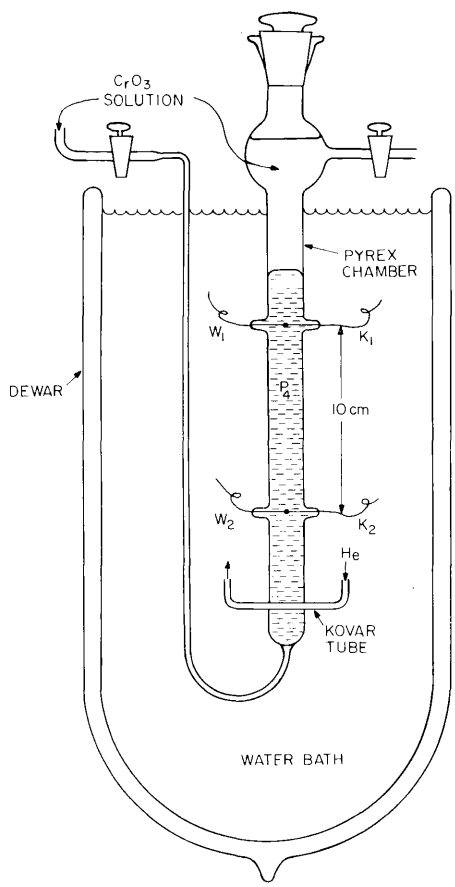

Fig. 7 - Apparatus for determining linear solidification rates in supercooled phosphorus. The surface of the P_4 specimen can be cleansed by periodically flushing CrO_3 solution through the apparatus.

A rate measurement was begun in the uniformly supercooled specimen by flushing a stream of cold helium gas through the Kovar tube that passed through the base of the 15-mm-diameter Pyrex column. The resulting rapid cooling chilled the P_4 specimen locally to the nucleation temperature; moreover, the chilling was applied so suddenly that no significant distortion was introduced into the uniform temperature field between the thermocouple junctions. The P_4 crystals that nucleated around the chilled Kovar tube spread rapidly through the supercooled specimen, and the abrupt change in temperature accompanying the solidification front was sensed, in turn, by junctions W_2/K_2 and W_1/K_1. Figures 8a and 8b are representative waveforms of the signal generated by the passage of the solidification front across the junctions of the differential thermocouple. The fast response achieved with this system (detectable signals within 1 millisecond) is attributed primarily to the small gauge of the tungsten and Kovar-A wires (0.005-in. diameter) and to the fact that since P_4 is an electrical insulator, no additional insulation was needed on the junctions.

The average speed of solidification was calculated as the ratio of the length of the growth path to the transit time measured from the waveform produced by the thermocouples. Figure 9 shows a logarithmic plot of the speed of solidification versus the degree of normalized supercooling prior to freezing. The most significant feature of these results is that no discontinuity in slope, or other peculiarity, occurred in the velocity-supercooling relationship as the system became hypercooled, i.e., as $\vartheta_e - \vartheta_0$ exceeded unity. It will ~~not~~ may be shown that interface temperatures can be estimated when solidification rates are known in the hypercooled temperature range, but considerable analysis is required to achieve this end.

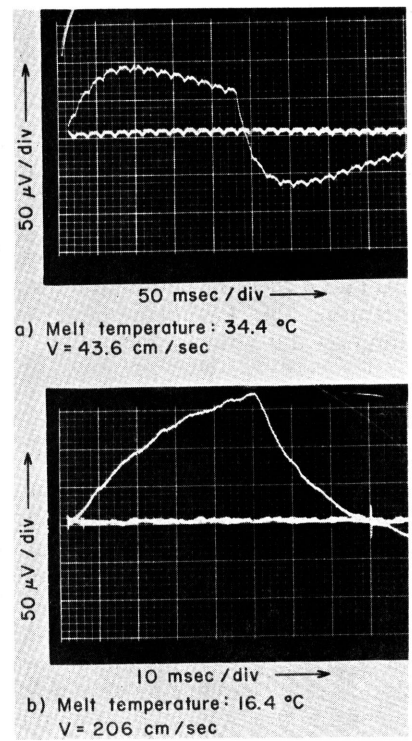

Fig. 8 - Representative waveforms of the output signal from the solidification-rate apparatus. The transit time for interface advance between the thermocouple junctions is taken as the interval between the "triggering" point of the waveform and the abrupt (negative) increase in slope. Transit times in phosphorus varied between 25 msec and 1 sec for the range of supercooling studied.

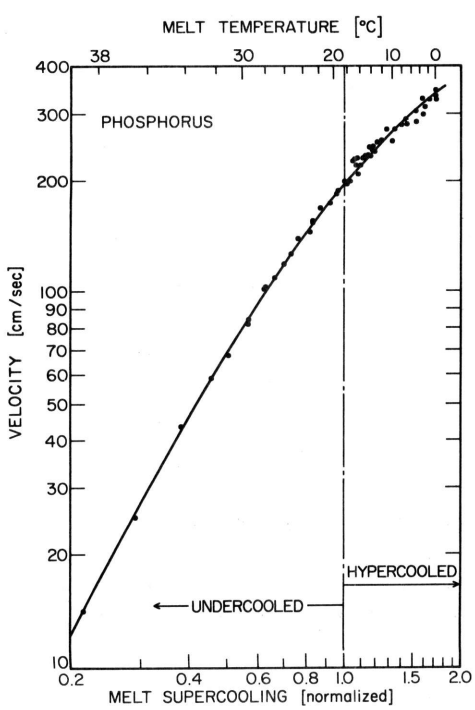

Fig. 9 - Velocity of the solidification front versus melt supercooling (lower abscissa) and melt temperature (upper abscissa). The curvature of the plot on a log-log scale indicates that no simple power-law relationship exists between V and $\Delta\vartheta$ over the range of $\Delta\vartheta$ investigated here.

DATA ANALYSIS

Planar Growth Hypothesis

Horvay and Cahn (12) have shown in a rigorous fashion that when a crystal grows into a uniformly supercooled melt, the *maximum* normalized temperature difference that can exist between the solid/liquid interface (assumed spatially isothermal) and its melt (far from the interface) is unity. Moreover, irrespective of interface morphology, if this normalized temperature difference, $\vartheta_i - \vartheta_0$ (see Fig. 3) approaches unity, then interface motion and shape become characterized by a Péclet number that approaches infinity. The Péclet number Pé is a convenient dimensionless heat-flow parameter defined by the relationship

$$\text{Pé} = \frac{Vr}{2\alpha} ,$$

where V and r are the normal velocity and mean radius of curvature of the interface, respectively, and α is the thermal diffusivity of the melt. V, of course, must always be finite, so a Péclet number approaching infinity implies that r is approaching infinity, or, equivalently, that the mean gaussian curvature of the interface is approaching zero. This general conclusion reached by Horvay and Cahn is formally equivalent to the specific result shown by Eqs. (1a) and (1b) in our discussion of planar isenthalpic solidification: viz., that a planar solidification front propagates through the melt with a unitary normalized temperature rise above the melt temperature, and that the planar solidification front is the most sluggish type of front insofar as a maximum amount of the available supercooling is used up in driving the heat transfer process. Since in our experiments we were able to achieve normalized supercooling levels as large as 1.7, the possibility must be considered that planar solidification could take place in P_4, with the true interface temperature as much as 18.4 C° (0.7 normalized) below the equilibrium temperature.

In planar solidification, where no Gibbs-Thompson effect occurs, the normalized supercooling δ responsible for kinetic processes (other than heat flow) is given by

$$\delta = \vartheta_e - \vartheta_i = \Delta\vartheta - 1. \tag{3}$$

A logarithmic plot of solidification speed V against $\Delta\vartheta - 1$ would either reveal the true dependence of V on δ (if the morphology was indeed microscopically planar) or prove, unequivocally, that the morphology was nonplanar even at extreme levels of supercooling. Theoretical works by Wilson (13), Frenkel (14), Hillig and Turnbull (15), and more recently, by Cahn (16) and by Cahn, Hillig, and Sears (17) have shown the existence of either a quadratic or linear relationship between V and δ, depending on whether interface motion occurred by lateral spreading of growth layers from dislocation sources, or by uniform advancement via random atomic attachment, respectively. Figure 10 indicates that neither a linear, quadratic, nor other simple power-law relation exists between V and $\Delta\vartheta - 1$. Instead, we conclude from these data that $\delta \neq \Delta\vartheta - 1$, and, therefore, that P_4 solidifies with a nonplanar (microscopically scalloped) interface even when the total supercooling is as large as 1.7. The presence of a nonplanar interface during solidification demands that both the Gibbs-Thompson effect and the effect of multidimensional heat flow be considered when attempting to deduce the interface kinetic relationship $[V = f(\delta)]$ from the experimental rate data $[V = g(\Delta\vartheta)]$.

Analysis for Nonplanar Growth

In the preceding section we proved indirectly that P_4 freezes with a nonplanar interface morphology from both undercooled and hypercooled melts. To proceed further with

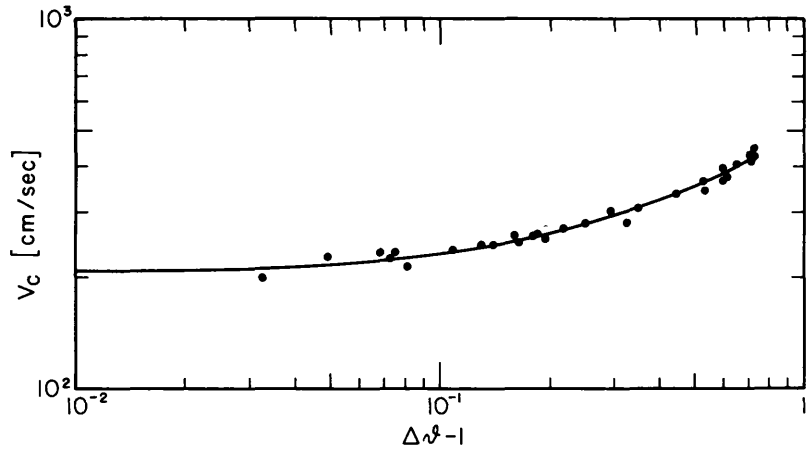

Fig. 10 - Growth velocity (corrected for viscosity) as a function of interface temperature $\Delta\vartheta - 1$, assuming, a priori, a planar interface morphology during growth from hypercooled melts. The absence of a linear or quadratic relationship between V_c and $\Delta\vartheta - 1$ indicates that no planar growth actually occurs.

an interface temperature determination, some estimate must be made of the shape of the solid/liquid interface in those regions* where the interface advances normal to itself most rapidly.

Phosphorus (α phase) is composed of rather symmetrical P_4 molecules arranged on a bcc lattice (18) with a large unit cell that contains 56 P_4 molecules (19). The rotations of the P_4 molecule remain unquenched in the solid phase down to low temperatures (196°K) (20,21) which accounts for phosphorus' low, typically metallic, entropy of fusion (1.98 cal/°K-mole P_4). In view of these properties, we believe that in P_4 the protuberances (dendrites or scallops) that constitute the nonplanar solid/liquid interface are similar to those found in metals (2). Moreover, we shall assume, *a priori,* that a paraboloidal surface adequately approximates the true shape of the protuberances over a limited region near their tips.

It has been shown by Bolling and Tiller (22) that an isothermal paraboloid cannot be a precise description of the state of an isolated growing dendrite; the sides of the dendrite have less curvature than the tip and grow more slowly, and must, therefore, be warmer than the tip. However, when we consider growth at large normalized supercoolings, adjacent protuberances will tend to warm the sides of one another and thus make more probable the propagation of approximately paraboloidal shapes with the required nonisothermal surface. In addition, Table 1 shows that for P_4 the ratio of the thermal diffusion length α/V to the critical radius for nucleation r^* is only about 14, over most

*The tip area of a dendrite or scallop is an example of these regions; in particular, note that measurement of solidification speed usually is confined to measurement only of tip speed.

of the range of experimentally attainable supercoolings. Since r* is the minimum radius possible for a dendrite tip, the small α/Vr^* values indicate that the *tip region* of any particular interface protuberance has a thermal environment that is not strongly affected by the thermal diffusion fields of similar neighboring protuberances, nor is it affected significantly by any shape instabilities developing behind the tip region (4). For these reasons, a tractable, yet not unreasonable, heat-flow analysis can be applied here, wherein the tip regions of the interface protuberances are considered as independently advancing paraboloids, the tip temperatures of which are not affected by the heat released by neighboring protuberances.

Table 1
Calculated Quantities for P_4

Super-cooling $\Delta\vartheta$	Critical Radius r* (cm × 10^7)	Thermal Diffusion Length α/V (cm × 10^5)	$\frac{\alpha}{Vr^*}$
0.2	27.5	12.3	45
0.4	13.8	3.2	23
0.6	9.2	1.5	16
0.8	6.9	0.91	13
1.0	5.5	0.78	14
1.2	4.6	0.63	14
1.4	3.9	0.53	14
1.6	3.4	0.47	14
1.7	3.2	0.46	14

Values of solidification speed were read from the smooth curve drawn through the V vs $\Delta\vartheta$ data in Fig. 9, at normalized supercooling values that conveniently covered the range of observation, viz., 0.2, 0.4, 0.6, 0.8, 1.0, 1.2, 1.4, 1.6 and 1.7. Each coordinate pair (V, $\Delta\vartheta$) formed the basis for a diagram such as shown in Fig. 11. Figures 11a and 11b relate normalized temperature differences to the tip radius of the paraboloidal protuberances which we assume describe the tip regions of the solid/liquid interface. The tip radii are, for convenience, expressed in units of the critical radius for nucleation.* The curves labeled GT, representing the difference between tip equilibrium temperature $\vartheta_e(r)$ and melt temperature ϑ_0 at infinity were calculated as a function of r/r^* with the Gibbs-Thompson equation,

$$\vartheta_e(r) - \vartheta_0 = \Delta\vartheta(1 - r^*/r);$$

see Fig. 3 for the definitions of each normalized temperature or temperature difference. The curves labeled HC represent the differences between normalized interface temperature ϑ_i and melt temperature ϑ_0 at infinity calculated from the Horvay-Cahn heat-flow equation (12) for circular paraboloids,

$$\vartheta_i - \vartheta_0 = -\text{Pé}[\exp(\text{Pé})]\,\text{Ei}(-\text{Pé}). \tag{4}$$

Although the temperature difference given by Eq. (4) is most conveniently expressed as a function of the Péclet number Pé it should be noted that the variables Pé and r/r^* are simply related through the identity

*Critical radii were calculated here on the basis of a solid/liquid surface energy of 8 erg/cm^2.

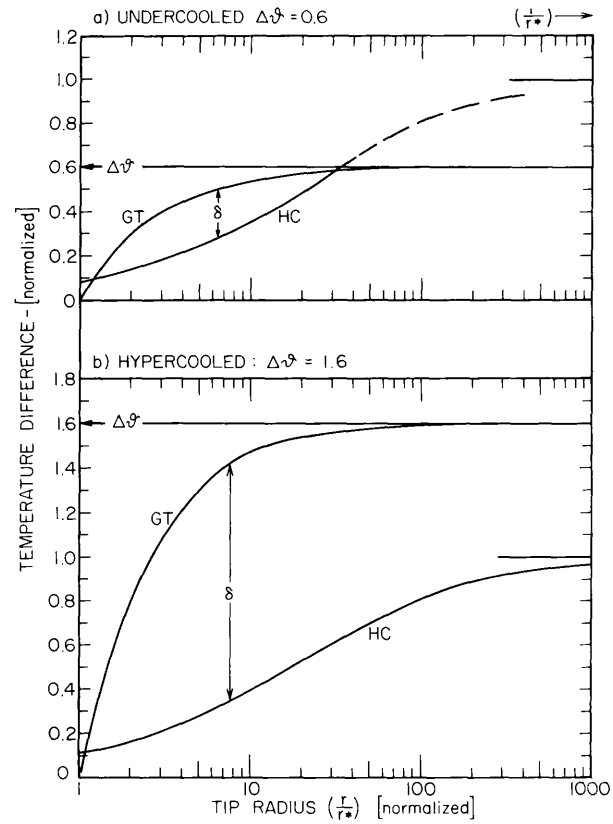

Fig. 11 - Temperature differences arising from curvature and heat-flow effects at the tips of advancing paraboloids, as functions of the tip radius. (a) Undercooled melt ($\Delta\vartheta$ = 0.6), showing finite range of acceptable values of r/r^* which give positive values of δ. (b) Hypercooled melt ($\Delta\vartheta$ = 1.6), showing a semi-infinite range of acceptable values of r/r^*. $\Delta\vartheta$ represents the position of the normal melting point relative to the temperature of the supercooled bath; the curves designated GT (Gibbs-Thompson) represent the local equilibrium temperature $\vartheta_e(r)$ as affected by the tip curvature; the curves designated HC (Horvay-Cahn) represent the rise of interface temperature ϑ_i above melt temperature, due to latent heat emission. The HC curves are based on the measured growth velocity observed in P_4 for each value of $\Delta\vartheta$. δ is the interfacial supercooling driving solidification kinetics.

$$\text{Pé} = \frac{Vr}{2\alpha} \equiv \frac{Vr^*}{2\alpha}\left(\frac{r}{r^*}\right),$$

where the specific constant of proportionality between Pé and r/r^* is again derived from the experimental values of V and $\Delta\vartheta$ upon which the particular diagram is based. Hence, each HC curve expresses $\vartheta_i - \vartheta_0$ as a function of r/r^*.

Since the ordinate difference between curves GT and HC represents exactly the normalized temperature difference δ responsible for "driving," at the tip, kinetic processes other than heat flow, it is clear then that Figs. 11a and 11b succinctly reveal the total range of solidification behavior consistent with our model and with experiment. In other words, for each coordinate pair (V, $\Delta\vartheta$) a specific range of tip radii is obtained over which solidification is possible, that is, over which nonzero, positive values exist for δ. A striking difference between the behavior of a normally undercooled melt (Fig. 11a) and a hypercooled melt (Fig. 11b) is that the solidification must occur over a limited range of r/r^* for the former, whereas a semi-infinite range of r/r^* is admissible for the latter.

Determination of Interface Temperature

Cahn, Hillig, and Sears have shown that the kinetics of atomic attachment at a solid/liquid interface can be displayed graphically by plotting $V[\eta(\vartheta_i)/\eta_0]/\delta$ versus δ, where the factor $\eta(\vartheta_i)/\eta_0$ is the ratio of the melt's viscosity at the interface temperature ϑ_i to the melt's viscosity at the normal melting temperature. Correction of the velocity by the ratio $\eta(\vartheta_i)/\eta_0$ compensates for the changes in the intrinsic solidification rate caused by changes in the self-diffusion rate with temperature in the region of the solid/liquid

interface. Of course, to apply their analysis we first must determine the particular value of δ or r/r^* (since δ is already a known function of r/r^*) which characterizes the P_4 system at each $(V, \Delta\vartheta)$ coordinate.

Figure 12 is a composite plot of $V[\eta(\vartheta_i)/\eta_0]/\delta$, henceforth denoted V_c/δ, versus r/r^* for various fixed values of the experimental coordinates $\Delta\vartheta$ and V. The self-diffusion corrections used in Fig. 12 are based on published values for the viscosity of P_4 (23,24). These corrections were calculated on the basis of the interface temperatures ϑ_i computed by the Horvay-Cahn analysis for each value of r/r^*, $\Delta\vartheta$, and V. The curves in Fig. 12 represent the possible combinations of V_c/δ and r/r^* which are consistent with the experimental measurements of V and $\Delta\vartheta$, and with the paraboloidal model of the solid/liquid interface. We see that the minimum values of V_c/δ all fall within a few percent of each other; that is, $(V_c/\delta)_{min}$ is approximately constant over a wide range of $\Delta\vartheta$. In addition, the curves drawn for the hypercooled melts indicate that the maximum* values of V_c/δ are decreasing with increased supercooling and, moreover, are approaching $(V_c/\delta)_{min}$.

Strictly speaking, the foregoing analysis provided only upper and lower limits for V_c/δ over the entire supercooled range. Fortunately, in P_4 we have found that the upper limit converged rapidly toward a nearly constant lower limit as $\Delta\vartheta$ increased. We conclude from this behavior that the values of $(V_c/\delta)_{min}$ are the characteristic values we seek to describe the solidification behavior of this system, and that the corresponding values of r/r^* represent the true tip radii of the dendrites or scallops. A satisfying aspect of this result is that without recourse to any *a priori* maximization principle we have found strong indications that P_4 solidifies with the maximum amount of interfacial supercooling consistent with the stipulated model for interface morphology. Solidification at maximum kinetic supercooling with a given $\Delta\vartheta$ is formally equivalent to solidification at maximum velicity with a given V_c/δ. However, since no legitimate theoretical basis exists for the maximum velocity principle (25), these results for P_4 are given only as empirical findings and not as a justification for the general applicability of any maximization principle. Obviously, this point requires additional theoretical review as well as further experimentation on other systems.

Interface Kinetics for P_4

If we accept, for the time, $(V_c/\delta)_{min}$ as the characteristic parameter for solidification in P_4, then the kinetic behavior can be represented conveniently by a plot of $(V_c/\delta)_{min}$ against δ, as shown in Fig. 13. The upper curve in Fig. 13 showing $(V_c/\delta)_{max}$ versus δ was added to emphasize the rapid convergence of this upper bound toward $(V_c/\delta)_{min}$ as δ increases. It is apparent from Fig. 13 that a linear dependence exists between V_c and δ, since $(V_c/\delta)_{min}$ is a constant (above $\delta \cong 0.1$). The value of this constant is 450 ± 10 cm/sec, corresponding to a rate constant of 17.7 ± 0.4 cm/sec C°. The linear relationship between V_c and δ implies that uniform attachment kinetics are controlling at the solid/liquid interface in P_4 when the melt supercooling $\Delta\vartheta$ is greater than about 0.35 (or on a dimensional scale, greater than about 9 C°). The data in Fig. 13 also show some indication of the onset of the so-called transitional growth regime below about $\delta = 0.1$. Below $\delta = 0.1$, the curve bends downward rather abruptly as the growth mechanism presumably changes from uniform attachment kinetics (linear in δ) to layer-passage limited kinetics (quadratic in δ).

*We specifically exclude from the present analysis the steeply rising values of V_c/δ at values of r/r^* near unity. Steady-state solidification at small r/r^* is considered physically untenable, insofar as the kinetic supercooling, δ, would be very unstable relative to any slight variations in interface curvature, which occur during solidification. Steady-state solidification requires a reasonably weak dependence of V_c/δ on r/r^*; for this reason, we do not believe that steady-state growth can occur with r/r^* near unity.

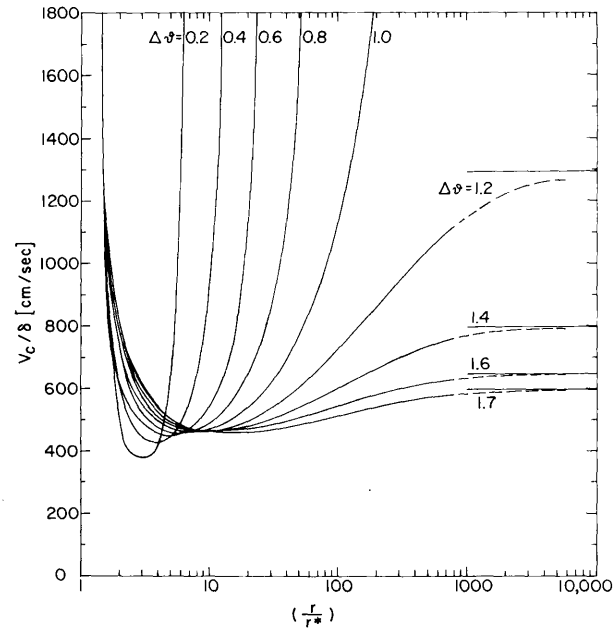

Fig. 12 - Curves showing V_c/δ as a function of r/r^*, for several values of the melt supercooling $\Delta\vartheta$. δ is calculated as in Fig. 11 by using the measured value of V corresponding to each $\Delta\vartheta$. Curves for $\Delta\vartheta \geq 0.4$ all show minimum values of V_c/δ at about 450 cm/sec. In addition, curves for $\Delta\vartheta > 1$ yield maximum values for V_c/δ at large r/r^*.

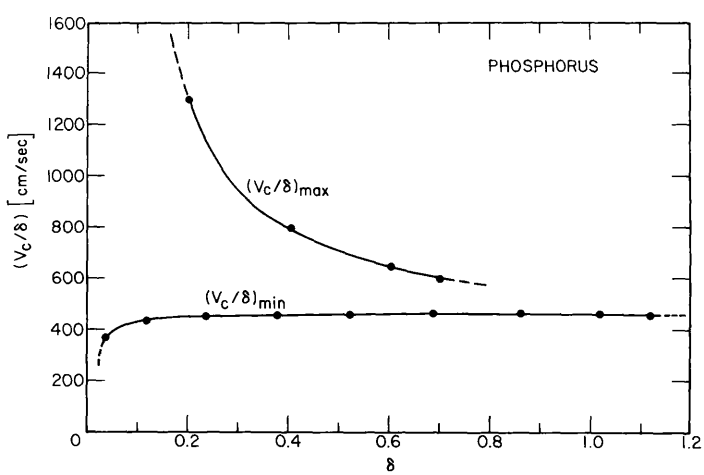

Fig. 13 - Minimum and maximum values of V_c/δ, from curves in Fig. 12, shown as functions of δ. Note that, as δ increases, the values of $(V_c/\delta)_{max}$ appear to approach the almost constant level of $(V_c/\delta)_{min}$. The convergence of $(V_c/\delta)_{min}$ and $(V_c/\delta)_{max}$ limits the uncertainty in the true value of (V_c/δ) to less than 30 percent. However, it is believed that $(V_c/\delta)_{min}$ is, in fact, the true value.

Our preliminary observations of solidification in P_4 at melt supercooling near 1 C° confirm the presence of faceted growth morphologies* at very low levels of supercooling. It seems clear, therefore, that somewhere in the range of melt supercooling between 1 C° and 9 C° the atomic mechanism of crystal growth in P_4 changes from layer spreading to uniform attachment. The present series of experiments are qualitatively explained by the molecular crystal growth theory of Cahn, Hillig, and Sears, and are not understood in terms of Jackson's theory (26) of smooth and rough interfaces — a theory which does not predict the observed change in growth mechanism with increased kinetic driving force.

In their paper, Cahn, Hillig, and Sears accepted the approximately quadratic relationship between V_c and $\Delta\vartheta$, which had been observed in P_4 by Powell, Gilman, and Hildebrand (27) as evidence for layer-passage limited (nonlinear) kinetics. Although the present experiments are in agreement with Powell, Gilman, and Hildebrand's observations, we see no merit in Cahn, Hillig, and Sears' justification that this quadratic relationship indicates nonlinear kinetics, or, equivalently, that the melt supercooling $\Delta\vartheta$ is nearly equal to the true interface supercooling δ. Our analysis has shown, instead, that δ and $\Delta\vartheta$ are related by rather involved formulas, and, as indicated in Fig. 14, δ and $\Delta\vartheta$ differ appreciably in magnitude in P_4. The complicated dependence of δ and $\Delta\vartheta$ indicated in Fig. 14 suffices to undermine any straightforward interpretation of the relationship between V_c and $\Delta\vartheta$ except, perhaps, at very low values of $\Delta\vartheta$ where, for faceted growth, the interface temperature might be approximated reasonably by the ambient temperature of the melt. Fortunately, the relationship determined between V_c and δ is interpreted

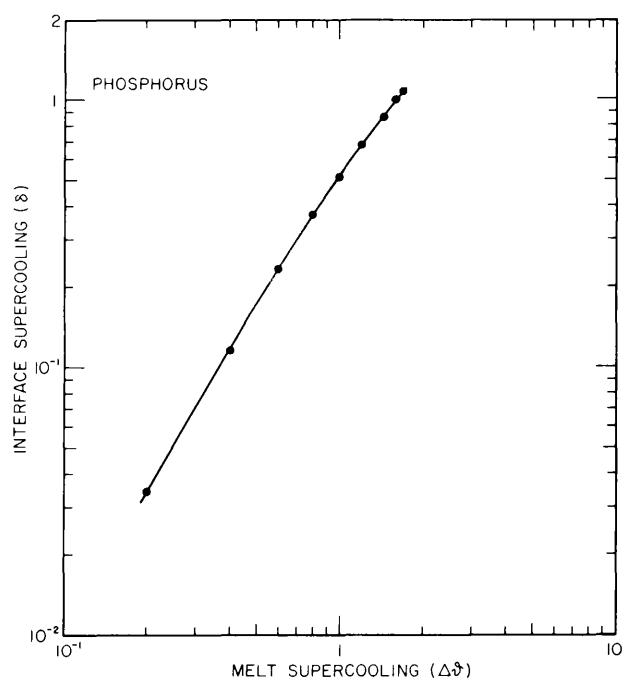

Fig. 14 - Relationship of interface supercooling δ [derived from $(V_c/\delta)_{min}$] to total melt supercooling $\Delta\vartheta$. The plot indicates that δ is considerably less than $\Delta\vartheta$ and that no simple relation exists between them.

*Faceted growth morphologies are strong evidence for layer-passage limited kinetics. See Ref. 17 for additional information on this point.

easily, except where transitional growth occurs at low values of δ. More work with P_4 is needed in the lower ranges of supercooling over which the atomic mechanism for crystal growth changes character.

Figure 15 shows the fractional distribution of total (melt) supercooling into its three components, δ, $\vartheta_i - \vartheta_0$, and $\vartheta_e - \vartheta_e(r)$. A surprising feature disclosed here is that the fractional supercooling for interface attachment processes $\delta/\Delta\vartheta$ rises rapidly with $\Delta\vartheta$ and accounts for more than half the total supercooling above $\Delta\vartheta = 0.9$. Even at the lower levels of supercooling for dendritic growth, δ accounts for more than 10 percent of the total.

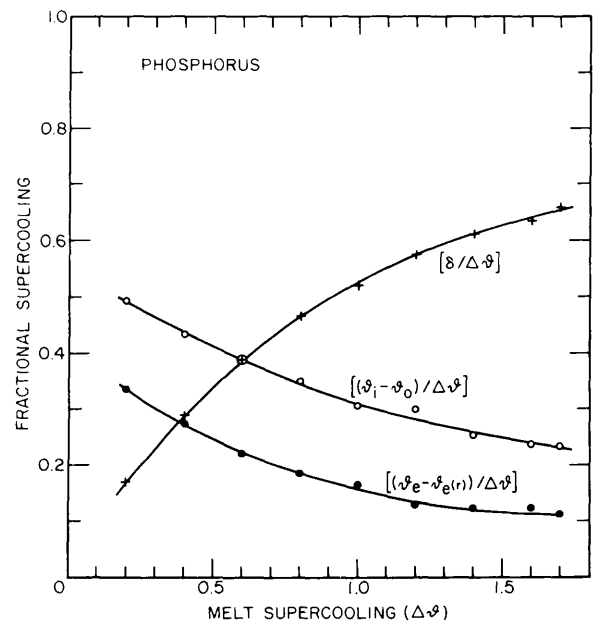

Fig. 15 - Fractional distribution of melt supercooling $\Delta\vartheta$ ascribed to kinetics $[\delta/\Delta\vartheta]$, heat flow $[(\vartheta_i - \vartheta_0)/\Delta\vartheta]$, and curvature $[(\vartheta_e - \vartheta_e(r))/\Delta\vartheta]$, as functions of $\Delta\vartheta$. Note the greatly increased importance of the kinetic contribution at large supercooling. The curves should not be extrapolated to supercoolings much below $\Delta\vartheta = 0.2$, because faceted growth becomes prevalent at low supercooling.

The fractional supercooling required for heat flow $(\vartheta_i - \vartheta_0)/\Delta\vartheta$ accounts for about half the total supercooling at low values of $\Delta\vartheta$, but only for about 25 percent at the larger values of $\Delta\vartheta$. Similarly, the fractional supercooling "lost" because of curvature effects $[\vartheta_e - \vartheta_e(r)]/\Delta\vartheta$ decreases from over 30 percent at small supercooling to a nearly constant 10 percent at large supercooling.

From the data in Fig. 15 we conclude that heat flow, attachment processes, and curvature effects individually represent important phenomena which collectively determine the overall solidification process in P_4; no one effect is extraordinarily dominant or rate limiting.

SUMMARY

1. The thermodynamic basis for univariant isenthalpic solidification has been discussed along with evidence for its occurrence in highly supercooled P_4.

2. Univariant isenthalpic solidification appears to be a unary-system analog to the solid-state reactions in binary alloys known as "massive" transformations.

3. Although plane-front solidification at constant speed is theoretically possible in hypercooled melts — because no long-range heat transport need occur — the actual morphology of the solid/liquid interface in P_4 remains essentially dendritic.

4. From observations on a macroscopic scale, it appears that a well-defined interface sweeps through the hypercooled system and "massively" transforms the melt to solid. However, on a microscopic scale the interface probably is composed of protuberances (scallops) which advance by release of latent heat into a multi-dimensional thermal diffusion field having a diffusion length on the order of only 10^{-5} cm. This type of heat flow is, most assuredly, more akin to dendritic behavior than to planar-front behavior.

5. Solutions to the time-independent heat-flow equation, developed by Horvay and Cahn for isothermal dendrites, were used in the present analysis with some modifications to account for the Gibbs-Thompson effect and the occurrence of appreciable interface supercooling. Our analysis indicates that P_4 solidifies in modes that maximize the interface supercooling for a given level of melt supercooling. Moreover, the data indicate that uniform attachment kinetics are rate controlling when P_4 solidifies with a normalized interfacial supercooling greater than about 0.1. The linear rate-constant for P_4 is estimated to be 17.7 ± 0.4 cm/sec C°.

6. Layer-passage limited kinetics, as evidenced by the appearance of faceted growth morphologies at small levels of supercooling ($\Delta\vartheta < 1$ C°), change over to uniform attachment kinetics somewhere in the range of melt supercooling between 1 C° and 9 C°.

7. The total supercooling available for solidification is distributed, in a rather complicated way, among the contributing effects of molecular attachment, heat flow, and interface curvature. No one effect appears to be extraordinarily dominant — at least in terms of the fractional supercooling expended on the particular effect. However, at large supercoolings molecular attachment accounts for the major share of the total supercooling, whereas at small supercoolings heat flow appears to be the largest effect as long as dendritic growth persists.

ACKNOWLEDGMENT

The authors are indebted to Dr. C. A. Mackliet, Metal Physics Branch, NRL, for his many helpful discussions and to the Material Sciences Division, Advanced Research Projects Agency, for their financial support of portions of this research.

REFERENCES

1. Thomas, L.J., and Westwater, J.W., Chem. Eng. Progr. Symp. Ser. 59:155 (1963)

2. Jackson, K.A., and Hunt, J.D., Acta Met. 13:1212 (1965)

3. Davies, V.deL., J. Inst. Metals 93:10 (1964-1965)

4. Glicksman, M.E., and Schaefer, R.J., Acta Met. 14:1126 (1966)

5. Hamilton, D.R., and Seidensticker, R.G., J. Appl. Phys. 34:1450 (1963)

6. Jakob, M., "Heat Transfer," New York:Wiley, p. 344, 1949

7. Horvay, G., "Modified Stefan Problem," General Electric Rept. 64-RL-3733M, Aug. 1964

8. Christian, J.W., "The Theory of Transformations in Metals and Alloys," London: Pergamon, p. 601, 1965

9. Hildebrand, J.H., and Rotariu, G.J., J. Am. Chem. Soc. 73:2524 (1951)

10. Jackson, K.A., "Growth and Perfection of Crystals," edited by R.H. Doremus, B.W. Roberts and D. Turnbull, New York:Wiley, p. 319, 1958

11. Glicksman, M.E., and Schaefer, R.J., J. Chem. Phys. 45:2367 (1966)

12. Horvay, G., and Cahn, J.W., Acta Met. 9:695 (1961)

13. Wilson, H.A., Phil. Mag. 50:238 (1900)

14. Frenkel, J., "Kinetic Theory of Liquids," New York:Dover, p. 413-426 (1955)

15. Hillig, W.B., and Turnbull, D., J. Chem. Phys. 24:914 (1956)

16. Cahn, John W., Acta Met. 8:554 (1960)

17. Cahn, John W., Hillig, W.B., and Sears, G.W., Acta Met. 12:1421 (1964)

18. Natta, G., and Passerini, L., Nature 125:707 (1930)

19. Corbridge, D.E.C., and Lowe, E.J., Nature 170:629 (1952)

20. Bridgman, P.W., J. Am. Chem. Soc. 36:1344 (1914)

21. Ibid., 38:609 (1916)

22. Bolling, G.F., and Tiller, W.A., J. Appl. Phys. 32:2587 (1961)

23. Dobinski, S., Bull. Intern. Acad. Poln. Sci. Classe Sci. Math. Nat., Ser. A:103 (1934-1938)

24. Campbell, A.N., and Katz, S., J. Am. Chem. Soc. 57:2051 (1935)

25. Cahn, John W., private communication

26. Jackson, K.A., "Liquid Metals and Solidification," A.S.M., Cleveland, Ohio, p. 174-186 (1958)

27. Powell, R.E., Gilman, T.S., and Hildebrand, J.H., J. Am. Chem. Soc. 73:2525 (1951)

This page intentionally left blank.

Security Classification

DOCUMENT CONTROL DATA - R & D

(Security classification of title, body of abstract and indexing annotation must be entered when the overall report is classified)

1. ORIGINATING ACTIVITY *(Corporate author)* Naval Research Laboratory Washington, D.C. 20390	2a. REPORT SECURITY CLASSIFICATION Unclassified 2b. GROUP

3. REPORT TITLE

INVESTIGATION OF SOLID/LIQUID INTERFACE TEMPERATURES VIA ISENTHALPIC SOLIDIFICATION

4. DESCRIPTIVE NOTES *(Type of report and inclusive dates)*
An interim report on one phase of the problem

5. AUTHOR(S) *(First name, middle initial, last name)*

M.E. Glicksman and R.J. Schaefer

6. REPORT DATE October 13, 1967	7a. TOTAL NO. OF PAGES 24	7b. NO. OF REFS 27
8a. CONTRACT OR GRANT NO. NRL Problem No. 63M01-10 b. PROJECT NO. RR 007-01-46-5408 c. d.	9a. ORIGINATOR'S REPORT NUMBER(S) NRL Report 6600 9b. OTHER REPORT NO(S) *(Any other numbers that may be assigned this report)*	

10. DISTRIBUTION STATEMENT

This document has been approved for public release and sale; its distribution is unlimited.

11. SUPPLEMENTARY NOTES	12. SPONSORING MILITARY ACTIVITY Department of the Navy (Office of Naval Research) Washington, D.C. 20360

13. ABSTRACT

Isenthalpic solidification of a pure supercooled liquid is shown to result in either a two-phase solid/liquid mixture in invariant equilibrium or a single-phase, totally solid material in univariant equilibrium, depending on the level of supercooling prior to solidification. The critical supercooling above which univariant equilibrium is obtained is large for metals (hundreds of centigrade degrees) but much smaller for certain molecular substances. Experiments on white phosphorus (alpha P_4) show that the critical supercooling (25.6 C°) can be reached, and exceeded, easily. Solidification rate measurements taken above and below the critical supercooling for P_4 show that the solid/liquid interface temperature varies smoothly with melt supercooling, although light-scattering experiments indicate that rapid changes occur in the extent of the dendritic zone as the critical supercooling is approached and exceeded.

A method for extracting interface attachment kinetics from solidification rate data was examined in detail and applied to our rate measurements on P_4. We find that above about 9 C° supercooling, P_4 solidifies with linear attachment kinetics having a rate constant of 17.7 ± 0.4 cm/sec C°. Below about 1 C° supercooling, P_4 solidifies with a faceted morphology indicative of layer-passage limited kinetics. Between 1 C° and 9 C° supercooling, transitional growth kinetics occur. These

(over)

DD FORM 1 NOV 65 1473 (PAGE 1)

S/N 0101-807-6801

Security Classification

14. KEY WORDS	LINK A ROLE	LINK A WT	LINK B ROLE	LINK B WT	LINK C ROLE	LINK C WT
Solid/liquid interface						
Undercooled state						
Hypercooled state						
Planar solidification						
Nonplanar solidification						
Invariant equilibrium						
Univariant equilibrium						
Interface supercooling						

results are in qualitative agreement with the crystal growth theory of Cahn, et al., which predicts that attachment kinetics should change as the driving force for crystal growth is varied by substantial amounts.